Published in final edited form as:

Adv Biosyst. 2017 August ; 1(8): . doi:10.1002/adbi.201700099.

Attenuation of Maladaptive Responses in Aortic Adventitial Fibroblasts through Stimuli-Triggered siRNA Release from Lipid-Polymer Nanocomplexes

Chad T. Greco[a], **Robert E. Akins**[b], **Thomas H. Epps III**[a,c], and **Millicent O. Sullivan**[a]

[a]Department of Chemical and Biomolecular Engineering, University of Delaware, Newark, DE 19716, USA

[b]Department of Biomedical Research, Nemours – Alfred I. duPont Hospital for Children, Wilmington, DE 19803, USA

[c]Department of Materials Science and Engineering, University of Delaware, Newark, DE 19716, USA

Abstract

Lipid-siRNA assemblies are modified with photo-responsive polymers to enable spatiotemporally-controlled silencing of interleukin 1 beta (IL1β) and cadherin 11 (CDH11), two genes that are essential drivers of maladaptive responses in human aortic adventitial fibroblasts (AoAFs). These hybrid nanocomplexes address the critical challenge of locally mitigating fibrotic actions that lead to the high rates of vascular graft failures. In particular, the lipid-polymer formulations provide potent silencing of IL1β and CDH11 that is precisely modulated by a photo-release stimulus. Moreover, a dynamic modeling framework is used to design a multi-dose siRNA regimen that sustains knockdown of both genes over clinically-relevant timescales. Multi-dose suppression illuminates a cooperative role for IL1β and CDH11 in pathogenic adventitial remodeling and is directly linked to desirable functional outcomes. Specifically, myofibroblast differentiation and cellular proliferation, two of the primary hallmarks of fibrosis, are significantly attenuated by IL1β silencing. Meanwhile, the effects of CDH11 siRNA treatment on differentiation become more pronounced at higher cell densities characteristic of constrictive adventitial remodeling *in vivo*. Thus, this work offers a unique formulation design for photo-responsive gene suppression in human primary cells and establishes a new dosing method to satisfy the critical need for local attenuation of fibrotic responses in the adventitium surrounding vascular grafts.

Table of Contents

Correspondence to: Thomas H. Epps, III; Millicent O. Sullivan.

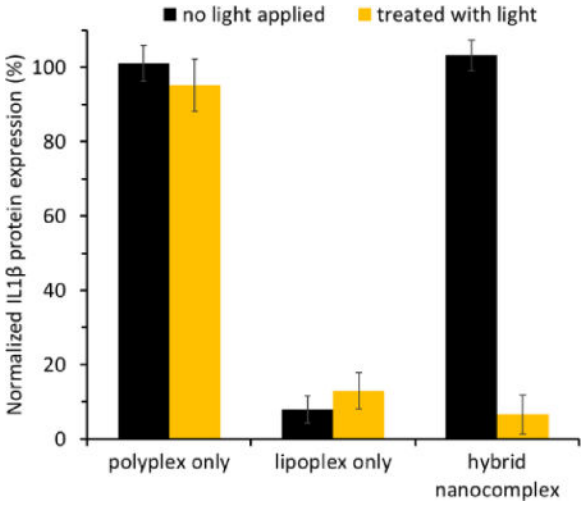

A lipid-polymer hybrid formulation is developed to spatiotemporally control the knockdown of IL1β and CDH11, two key genes implicated in maladaptive responses of human primary adventitial fibroblasts. The combined silencing of these genes for one week completely halts differentiation and significantly reduces proliferation, which are critical goals for treating fibrotic responses in injured cardiovascular disease.

Keywords

cardiovascular disease; bypass grafts; myofibroblasts; TGF-β1; block copolymers; photo-responsive; polyplexes

1. Introduction

Cardiovascular disease is the leading cause of death worldwide,[1] and vascular reconstructive surgeries, including the placement of bypass grafts, have become routine procedures for treating these ailments.[2] Unfortunately, even standard treatments, such as autologous vein grafts from the leg or arterial grafts from the arm or thorax, commonly fail within a few years due to inappropriate vessel remodeling.[3] These graft failures are primarily driven by maladaptive cellular responses elicited by tissue injury and hemodynamic stress.[4] Anastomoses, the sites of surgical vessel connection, are at particular risk due to suture line scarring, stricture, and higher incidences of stenosis and fibrosis.[5] Unfortunately, although drug eluting stents and externally applied films have shown promise in preventing complications, these interventions provide inadequate spatial and temporal control over cell behaviors in the graft conduit.[6] Thus, new methods are needed that can locally target the key cell types involved in failure. Such approaches could enable improved healing responses by tuning the application and release of regulatory therapies according to the localized environment within the site of injury.[7]

Adventitial fibroblasts (AFs), which populate the outermost layer of arteries, are particularly important cellular mediators of normal and pathogenic vessel remodeling.[8] Specifically, AFs are the dominant cell type in the adventitium, and they regulate the structural integrity

and growth of blood vessels through the production of extracellular matrix and the recruitment of the microvascular blood supply.[8b, 9] AFs contribute to the injury response through a variety of mechanisms, including their capacity to rapidly proliferate and differentiate into myofibroblasts, which have the ability to generate high contractile forces though the expression of alpha smooth muscle actin (αSMA) and the formation of multicellular networks.[10] Although such forces are necessary to induce vessel remodeling, this behavior is detrimental when it becomes excessive following reconstructive surgery.[11] In particular, AF proliferation and differentiation directly control the progression of intimal hyperplasia and fibrosis, leading to the accumulation of fibrous connective tissue, vessel thickening and scarring, and ultimately, graft failure.[7, 12] Therapeutic approaches geared toward the attenuation of AF-driven fibrosis would be extremely valuable.[10a] In fact, recent studies show significant promise for modulating adventitial responses through local application of biomaterials, such as hydrogels, to the abluminal surface of skeletonized vessels (*e.g.*, contacting adventitium), a procedure which was shown to reverse a series of adverse vessel remodeling responses to mechanical injury when the materials were applied during the acute inflammatory phase of post-surgical recovery.[13]

In addition to the local targeting of AFs through biomaterials application, the control of genes that regulate maladaptive responses in AFs also is critical to promote healing at anastomotic sites. For example, recent studies have elucidated key proliferative effectors and phenotypic modulators that likely play significant roles in the fibrotic response of AFs.[14] Two prominent genes noted in the above studies are interleukin 1 beta (IL1β), a cytokine that mediates injury-induced inflammation,[15] and cadherin 11 (CDH11), a cell-cell adhesion receptor that coordinates the contraction of fibroblast populations.[16] It also is important to understand the differential effects of IL1β and CDH11 on the signaling cascade initiated by transforming growth factor beta 1 (TGF-β1), a potent activator of myofibroblasts that is produced by local inflammatory cells and overexpressed in diseased environments.[17] Although TGF-β1-induced changes in both IL1β and CDH11 expression have been correlated with myofibroblastic differentiation and inflammation in fibroblastic lineages, the functional relationship between IL1β and CDH11 has not been explored in the context of adventitial remodeling.

Herein, we modified lipid-small interfering RNA (siRNA) complexes (lipoplexes) with stimuli-responsive polymers to gain spatiotemporal control over gene knockdown in human primary aortic adventitial fibroblasts (AoAFs), which enabled the elucidation of the functional roles of IL1β and CDH11 in improving vascular healing. These hybrid nanocomplexes were necessary because primary cells (*e.g.*, AoAFs) tend to be refractory to transfection compared to immortalized cell lines.[18] Moreover, our previous work established other beneficial properties of our mPEG-*b*-poly(5-(3-(amino)propoxy)-2-nitrobenzyl methacrylate) [mPEG-*b*-P(APNBMA)] block copolymer system for vascular applications, including high stability and the capacity to locally regulate the extent of protein silencing on cellular length scales.[19] Such features make our nanocomplexes ideal for incorporation into biomaterials, such as abluminally-applied hydrogels, to enable regulation of adventitial cell behavior through a combination of mechanical stimulation and spatial regulation of gene expression in anastomoses. Additionally, the precisely controlled nature of the system allows for accurate predictions of siRNA dosing regimens that facilitate gene

knockdown over clinically-relevant timescales associated with adventitial remodeling (one week).[20]

We exploited these characteristics through the formulation of hybrid nanocarriers that mediated on-demand, spatially-controlled knockdown of IL1β and CDH11 in AoAFs to ≤ 5% of their initial levels following treatment with a photo-stimulus. The silencing of IL1β on its own significantly reduced myofibroblast differentiation and proliferation, whereas CDH11 silencing on its own had only a moderate effect. Subsequently, kinetic modeling approaches were used to design dosing regimens that fully silenced IL1β and/or CDH11 together, over sustained time periods. Complete attenuation of TGF-β1-induced myofibroblast differentiation was achieved by simultaneously silencing IL1β and CDH11 for one week, the timescale relevant to adventitial remodeling.[20] Thus, we uncovered synergistic functional roles of IL1β and CDH11 in AoAFs and showed that sustained knockdown of these genes is a viable method for mitigating fibrotic responses. In the longer term, the photo-sensitive lipid-polymer nanocomplexes offer a unique opportunity to locally regulate fibrotic conditions in anastomoses and improve healing following cardiovascular surgery.

2. Results and Discussion

2.1 Hybrid nanocomplexes enable on/off control over gene silencing

To achieve spatially-tailored and temporally-tuned gene silencing in AoAFs, various formulations of polymer-only-siRNA complexes (polyplexes) were tested that had previously been shown to provide efficient, light-triggered siRNA delivery in murine embryonic fibroblasts.[21] None of the polyplex formulations were able to mediate efficient gene silencing in AoAFs (Figure 1). We suspected that a lack of endosomal escape might be the limiting factor, based on prior evidence demonstrating that human primary cells often are refractory to transfection.[18] Lipoplexes comprised of Lipofectamine RNAiMAX were shown to transfect AoAFs efficiently (Figure 1), presumably because cationic lipids can interact with endosomal membranes and enhance cargo escape in primary cells.[22] However, these lipid solutions were not capable of mediating photo-controlled, spatiotemporal release. In contrast, hybrid nanocomplexes combining lipids and polymers remained dormant in the absence of a photo-trigger but rapidly released siRNA following the application of light, leading to efficient gene silencing in AoAFs (Figure 1). The model gene, IL1β, was knocked down to ~5% of the protein expression levels measured in untreated controls, demonstrating that the hybrid siRNA nanocarrier system was vital to overcoming the shortcomings of the individual polyplex and lipoplex formulations. Moreover, the on/off control over siRNA activity afforded by the hybrid nanocomplexes can be easily extended to spatially regulate gene expression at cellular length scales using previously described procedures.[19, 23]

The hybrid nanocomplexes were formulated according to the process depicted in Figure 2. First, siRNA was complexed with a cationic lipid, Lipofectamine RNAiMAX. Because these lipoplexes possessed a net positive charge and the mPEG-*b*-P(APNBMA) also was cationic, an anionic component was needed to facilitate electrostatic interactions. Poly(acrylic acid) [PAA], a polymer with a high anionic charge density,[24] was mixed with the lipoplexes to

reverse the overall charge. Finally, the cationic mPEG-*b*-P(APNBMA) was incorporated to impart photo-responsive characteristics (charge reversal) to the system.

The structural design and formulation process of the hybrid nanocomplexes share similarities with other lipid-polymer systems in the literature.[25] Generally, polymers are added to lipid-based carriers to impart a specific characteristic to the system. These features include reduced charge, stealthy behavior, biocompatibility, smaller sizes, and enhanced endosomal escape.[26] Although these modifications have proven to be effective, few stimuli-responsive components have been used to induce controlled siRNA release within hybrid lipid-polymer assemblies.[27] Herein, mPEG-*b*-P(APNBMA) was used to gain photo-responsive control over the disassembly of lipid-containing complexes. This favorable combination of behaviors (*e.g.*, light-responsiveness and endosomal escape) presumably arose as a result of polymer shielding of the endosome-destabilizing cationic lipids prior to light-triggered polymer cleavage/charge reversal, which then initiated lipid-mediated endosome destabilization.[28] Thus, our nanocomplexes provide the benefits of both lipids and stimuli-sensitive polymers, enabling precisely tuned on/off control over nucleic acid activity in human primary AoAFs.

It is important to note that the composition of the nanocomplexes was optimized to transfect human AoAFs. Gene silencing experiments in similar cell types, such as fibroblasts from other species and/or other tissue origins, demonstrated the cell specificity of the nanocomplexes and suggested that the effects of protein knockdown would be minimal in other mesenchymal cells found in adventitium (Figure S1). The selective transfection of different cell types is a critical potential advantage of our approach. Furthermore, the composition of the multi-component, highly modular hybrid nanocomplex system can be easily tailored to enable improved cell specificity and avoid off-target effects.

2.2 Characterization of hybrid nanocomplexes

The hybrid lipid-polymer nanocomplexes were characterized to determine their fundamental physicochemical properties. As shown in Table S1, the nanocarriers had an average diameter of 168 nm, which is within the size regime of nanoparticles that are able to undergo endocytosis and enter cells.[29] The nanocomplexes had a zeta potential of +3.1 mV (Table S1), indicating that the nanocarrier surface was slightly positively charged but close to neutral. The relatively neutral zeta potential suggests that the mPEG-*b*-P(APNBMA) polymers were coating the lipoplexes and that the PEG chains were forming an outer corona around the charged cores.[30] The slight positive charge is favorable for inducing cellular uptake while minimizing interactions with serum-components.

Another important consideration in the formulation of new siRNA delivery vehicles is their cytotoxicity, especially when treating sensitive human primary cells such as AoAFs. As shown in previous work, mPEG-*b*-P(APNBMA)-only polyplexes did not lead to any significant change in cell viability relative to untreated cells (Figure S2).[28] The hybrid nanocomplexes also possessed excellent biocompatibility (~98% cell viability), similar to the previously-reported polyplexes.[28] AoAFs that were treated with mPEG-*b*-P(APNBMA)-only polyplexes or the hybrid nanocomplexes combined with the photo-stimulus exhibited a modest (~20%) decrease in cell viability compared to untreated cells,

indicating that 365 nm light was moderately cytotoxic. However, lipoplexes comprised of Lipofectamine RNAiMAX were significantly more cytotoxic than the polyplexes or the hybrid nanocomplexes, as treatment with lipoplexes reduced cell viability by ~18% and ~46% without and with 365 nm light, respectively (Figure S2). The lack of a significant cytotoxic response of the hybrid lipid-polymer nanocarriers further supports that the biocompatible mPEG-*b*-P(APNBMA) forms a corona that shields the cationic lipids from interacting with cells. This shielding feature, and its resulting low cytotoxicity, suggest that the hybrid nanocomplexes hold greater promise for use in therapeutic settings.

Finally, the light-triggered siRNA release behavior of the nanocomplexes was explored to gain a better understanding of the on/off gene silencing response. As shown in Figure S3, nanocarriers that were not irradiated with light remained stable and encapsulated nearly 100% of the siRNA. Nanocomplexes that were treated with the photo-stimulus for increasing lengths of time exhibited increasing amounts of siRNA release. After 10 min of irradiation, which is the dosage of light used during transfections, ~56% of the siRNA was released. The high level of light-triggered siRNA release helps explain the efficient, on/off gene silencing trends detected in cells, even when low concentrations of siRNA (10 nm) were used.

2.3 Gene silencing dynamics following a single siRNA dose

Given the controlled release nature of the nanocomplexes, the dynamics of protein knockdown were investigated to determine how to appropriately dose siRNA in AoAFs. Two genes implicated in maladaptive responses, IL1β and CDH11, were studied using a combination of experimental analyses and kinetic modeling. siRNAs targeting IL1β or CDH11 were delivered to cells using the nanocomplexes, and siRNA release was induced upon application of a photo-stimulus at 3.5 h post-transfection. According to the model, protein expression for both genes was expected to decrease immediately following photo-induced siRNA release (Figure 3A). However, the rate of change in protein concentrations varied between the two genes. IL1β protein expression was forecasted to be almost fully knocked down ~16 h post-transfection, whereas complete CDH11 knockdown was not expected until ~27 h post-transfection. The proteins were predicted to be silenced to ≤ 5% of their initial levels for ~47 h (IL1β) or ~34 h (CDH11) before recovering. Experimental measurements of protein concentrations taken at various times validated these predictions and demonstrated that the model could accurately capture all three phases of the gene silencing process – *e.g.*, initial knockdown, maximal silencing, and recovery of protein expression.

The protein silencing dynamics for IL1β and CDH11 followed the same overall trend, expect that the rate of initial protein knockdown depended on the half-lives of the two proteins (IL1β and CDH11 have protein half-lives of ~2.5 h and ~8 h, respectively).[31] If sufficient amounts of siRNA are released to saturate the RNA-induced silencing complex machinery, the cleavage of targeted mRNAs rapidly occurs, and the translation of new protein is halted. The existing protein, translated before the onset of RNAi initiation, would then degrade in time according to its innate turnover rate. Therefore, the concentration of IL1β should decrease faster than CDH11 on the basis of its shorter protein half-life.

On the other hand, the duration of sustained maximal silencing depends more strongly on the doubling time of the cells, and to a much lesser extent, upon the stability of the siRNA.[32] The intracellular siRNA is diluted in time due both to cell division and degradation from nucleases, and RNAi effects generally only last for a few days in growing cells, such as AoAFs. The concentration of IL1β- and CDH11-targeted siRNA in the AoAFs decreased at approximately the same rate, and the protein levels start to recover at ~3 days post-transfection as detailed by the modeling and experimental data. Thus, these analyses elucidated the dynamics of IL1β and CDH11 knockdown in AoAFs following a single dose of siRNA. These timescales are consistent with those for inflammation-mediated fibroblast proliferation,[8a, 13] providing further justification for the use of IL1β- and CDH11-targeted siRNAs for the treatment of cardiovascular disease.

2.4 Gene silencing dynamics following a double dose of siRNA

Following severe injury, adventitial remodeling/myofibroblast differentiation occurs over a time period of ~7 days,[20] and thus, sustained gene silencing is needed in such cases. Our kinetic modeling allowed the implementation of dosing schedules that enabled knockdown below a desired threshold over the one week duration. More specifically, using the framework established in Figure 3A, different dosing regimens were analyzed to predict the RNAi response following a second application of siRNA. As shown in Figure 3B, the second transfection was started at 72 h; i.e. near the time at which the protein levels were predicted to start recovering after the first transfection. The model forecasted that implementation of this dosing schedule would allow the knockdown of both genes to be sustained for ~7 days at levels of < 20% relative to untreated controls. Experimental measurements of protein levels validated this dosing regimen model and demonstrated that the predictions accurately captured the prolonged knockdown and recovery phases. Thus, our modeling approach allowed us to accurately predict that only two doses were needed to achieve gene silencing of both genes over the clinically-relevant timescale of one week.[13] Intriguingly, the relevance of this timescale for modulation of longer-term fibrotic responses was recently demonstrated by Robinson *et al.*, who reported that vessels subjected to common surgical procedures used during grafting (*e.g.*, skeletonization) displayed multiple maladaptive tissue responses within 3 days of surgery, with decreases in cyclic strain stabilizing within ~1 week.[13] In this model, acute abluminal application of thin (~1 mm) and mechanically-tunable hydrogels reversed fully many of the adverse responses to surgery. The addition of light-responsive nanocomplexes to such materials could provide a compelling approach to further tune and suppress failure responses, particularly in anastomoses or other regions of the graft tissue experiencing high mechanical stress.

One challenging aspect of implementing predictive siRNA dosing schedules is the effect of the silenced genes on cellular parameters governing responses to subsequent siRNA applications. Proliferation analyses (discussed later) determined that the knockdown of IL1β slowed cellular growth rates by ~30% after each dose. Thus, the kinetic model was updated with this information to account for the change in siRNA dilution rate as a result of a longer cell doubling time. The updated model accurately predicted that IL1β would remain knocked down longer than CDH11, which was verified by experimental measurements.

Therefore, the combination of a double dosing regimen and simple kinetic modeling enabled the knockdown of both genes to be sustained for one week in a predictable manner.

2.5 Gene silencing affects myofibroblast differentiation (αSMA protein expression)

One of the primary hallmarks of fibrosis is the differentiation of fibroblasts into myofibroblasts, which is driven by the production of TGF-β1 by local inflammatory cells.[15] Accordingly, to simulate the inflammatory fibrotic responses in culture, recombinant TGF-β1 protein was added to the growth medium of AoAFs. The cells were treated with formulations of non-targeted siRNA, IL1β siRNA, CDH11 siRNA, or combined IL1β and CDH11 siRNAs *via* the single dosing schedule in Figure 3A. The extent of differentiation was determined by measuring changes in αSMA protein expression, the most widely used indicator of the myofibroblast phenotype.[4, 8a] As shown in the micrographs in Figure 4A, the addition of TGF-β1 induced AoAFs to differentiate into myofibroblasts within 3 days, consistent with responses reported in the literature.[33] Specifically, AoAFs that were not treated with TGF-β1 expressed low levels of αSMA protein relative to F-actin protein; however, cells treated with TGF-β1 and either no siRNA or a single dose of non-targeted siRNA exhibited robust αSMA protein expression.

AoAFs treated with TGF-β1 followed by application of functional siRNAs targeting IL1β exhibited a significant reduction in αSMA staining, indicating that knocking down IL1β blocks the differentiation cascade to a measurable extent. In contrast, TGF-β1-treated cells with silenced CDH11 maintained robust αSMA protein expression. AoAFs that were treated with both IL1β and CDH11 siRNAs also exhibited decreased αSMA staining. The quantification of protein expression based upon these immunocytochemistry (ICC) experiments is shown in Figure 4B and is presented as αSMA relative to F-actin. As can be noted from the micrographs, αSMA protein expression was only significantly attenuated when IL1β was knocked down (either alone or in combination with CDH11) using the single dose regimen.

To determine how myofibroblast differentiation would be affected by the double dosing regimen, αSMA protein expression was analyzed on day 8. The differences in protein expression as a function of IL1β and/or CDH11 knockdown were more prominent in the double dosing experiments, though the overall trends were similar to the single dosing studies (comparison of Figures 4B and 4C). The delivery of IL1β siRNA suppressed αSMA levels by ~45% at day 8 relative to treatment with non-targeting siRNA. However, CDH11 silencing alone provided no reduction in αSMA protein expression compared to treatment with non-targeting siRNA. This behavior most likely was exhibited because AoAFs that were treated with only CDH11 siRNA had differentiated to approximately the same extent as cells treated with non-targeting siRNA before application of the second dose (Figure 4B), and further CDH11 knockdown could not reverse the myofibroblast phenotype. A recent report demonstrated that the de-activation of myofibroblasts is difficult to control and that the restricted capacity of myofibroblasts to de-differentiate is a major cause of fibrotic disorders.[34]

Regardless of dosing regimen, only cells treated with IL1β siRNA exhibited a significant reduction in αSMA protein expression (Figure 4). In agreement with our findings, Guo *et al.*

demonstrated that the neutralization of IL1β *in vivo* attenuated fibrosis and was correlated with decreases in TGF-β1 activity.[35] A number of recent studies also reported that increased IL1β levels enhanced the severity of fibrosis *in vivo*.[36] In a related example, Chen and coworkers showed that IL1β-stimulation of HO-8910PM and NIH3T3 cells increased the expression of αSMA and activated proteins involved in myofibroblast differentiation.[37] However, others have reported different impacts of IL1β activity on αSMA expression in other cell types,[15, 38] and moreover, Dewald *et al.* found significant species-specific differences in cellular responses to inflammatory cytokines following myocardial infarction.[39] Our finding that IL1β silencing effectively blocked TGF-β1-induced αSMA protein expression in AoAFs is likely applicable to fibroblasts derived from different organs but may not directly translate to all cell types or species.

CDH11 silencing in AoAFs did not attenuate αSMA protein expression compared to treatment with non-targeting siRNA, and the combination of CDH11 and IL1β silencing also did not further reduce αSMA protein expression as compared with samples treated with IL1β siRNA only (Figure 4). The knockdown of CDH11 has been shown to regulate the myofibroblast phenotype differently depending on the cell type.[40] For example, Verhoekx *et al.* reported that αSMA expression remained unchanged in human dermal fibroblasts, but was reduced by ~50% in Dupuytren's myofibroblasts following CDH11 silencing.[40b] Wang and coworkers also found that CDH11 knockdown did not affect differentiation when porcine valvular interstitial cells were treated with 5 ng mL^{-1} of TGF-β1.[17] Moreover, because the activity of CDH11 is dependent on the number of cell-cell contacts, differences in cell density also may contribute to the variations in cellular responses (discussed later).

2.6 Gene silencing affects myofibroblast differentiation (αSMA mRNA expression)

To gain a more quantitative understanding of temporal differences in myofibroblast differentiation, changes in the mRNA transcript levels also were analyzed. As shown in Figure 5A, the trends for the single dosing regimen were generally in agreement with the ICC data from Figure 4B. In particular, the addition of TGF-β1 induced a six-fold increase in αSMA transcripts, and the knockdown of IL1β provided a significant decrease in differentiation. The combined knockdown of IL1β and CDH11 lead to a greater attenuation of αSMA mRNA expression than IL1β knockdown alone, although the αSMA levels were still higher than the 'no TGF-β1' control. CDH11 knockdown resulted in a minor, but statistically significant, reduction of αSMA transcript levels relative to cells not treated with siRNA. Despite slight differences, the measurements of αSMA mRNA (3 days) and αSMA protein expression (4 days) post-transfection, respectively, were in agreement.

The αSMA transcript levels also were studied on day 7 of the double dosing schedule. AoAFs incubated in TGF-β1 exhibited ~4.5 times more αSMA mRNA transcripts than untreated cells (Figure 5B), suggesting that untreated cells did not significantly alter their fibroblast phenotype on tissue culture plastic over 7 days (Figure S5). The delivery of IL1β siRNA significantly reduced αSMA mRNA levels relative to the delivery of non-targeting siRNA, whereas CDH11 silencing did not provide these effects. However, the combined knockdown of IL1β and CDH11 attenuated αSMA mRNA expression to the same level as

the no TGF-β1 control, indicating that differentiation was completely halted over one week with the double dosing schedule.

Given the lack of response from CDH11 silencing alone, the significantly enhanced attenuation of differentiation from the combined delivery of IL1β and CDH11 siRNA in comparison to IL1β siRNA alone (*i.e.*, combined effects that were more than simply additive) suggests that the two genes may cooperate synergistically. Little is known about the direct relationship between IL1β and CDH11, but Yoshioka *et al.* recently reported that the knockdown of CDH11 reduced IL1β-induced proliferation by 42% in rheumatoid arthritis-derived synovial fibroblast cells.[41] The authors concluded that CDH11 is involved in IL1β-mediated pathways, and that there is an indirect interplay between the two genes *via* β-catenin.[41] In a related study, Chang and coworkers demonstrated that CDH11 engagement had strong synergies with IL1β signaling upon interleukin 6 (IL-6) induction in synovial fibroblasts, and that the mitogen-activated protein kinase (MAPK) [c-Jun N-terminal kinase (JNK) and extracellular signal–regulated kinase 1 and 2 (ERK1/2)] and the nuclear factor kappa-light-chain-enhancer of activated B cells (NF-κB) pathways were activated.[42] Thus, the signaling cascades of IL1β and CDH11 may be related through β-catenin, MAPK, and/or NF-κB in AoAFs. These reports suggest that the two genes affect one another in other cell types,[43] but more work is needed to probe the intricate interactions between the downstream effectors of IL1β and CDH11 in AoAFs. However, our data strongly suggest that the combined knockdown of the two genes provides a powerful synergistic method for attenuating TGF-β1-induced myofibroblast differentiation.

2.7 Attenuation of cellular proliferation following gene silencing

In addition to myofibroblast differentiation, increased cellular proliferation is a classic hallmark of fibrosis. The reduction of fibroblast proliferation is a critical therapeutic goal to mitigate maladaptive responses and promote healing in cardiovascular tissues, particularly in the first week following vessel injury.[8a, 44] Changes in the growth rates of the AoAFs were analyzed to determine if the knockdown of IL1β and/or CDH11 affected proliferation. As shown in Figure 6, non-targeting siRNA did not significantly alter proliferation, which is indicative of the biocompatibility of the hybrid nanocomplexes. The knockdown of IL1β reduced proliferation by ~30% and ~50% following a single and double dose, respectively. The delivery of only CDH11 siRNA provided a relatively minor reduction in proliferation rate in comparison to the untreated control samples. The combined knockdown of IL1β and CDH11 reduced proliferation to the same extent as IL1β alone. Thus, IL1β, but not CDH11, appears to play a critical role in AoAF proliferation.

Our findings in AoAFs are generally in agreement with most literature reports of IL1β and CDH11 in other cell types.[37, 41, 45] While IL1β has been widely identified as playing a key role in fibroblast proliferation, few studies have implicated CDH11.[41] For example, Vesey *et al.* found that IL1β was a potent inducer of proliferation with similar activities to those of TGF-β1 in human cortical fibroblasts.[45] Consistent with these findings, our studies indicated that the synergistic effects of knocking down IL1β and CDH11 attenuated differentiation (Figure 5) but were not detected in the AoAF proliferation analyses.

2.8 Cell density effects on CDH11 knockdown

In both the single dose and double dose studies, the knockdown of CDH11 provided only minor, if any, attenuation of myofibroblast differentiation. However, previous work identified CDH11 upregulation in inflamed AoAFs as a primary marker of myofibroblasts,[14a, 16] thus making it a promising target for mitigating differentiation. One possible reason for this discrepancy is that CDH11 signaling requires cell-cell adhesion,[16] which occurs at high cell densities,[17] yet under standard culturing conditions, cell-cell contacts are not made until confluency (3–4 d in our study). Within the context of Figure 3B, CDH11 may be a better target after day 3 when the cells are beginning to become more confluent. A second possible explanation is that CDH11 is simply a downstream effector of other proteins that govern the differentiation pathway, and the modulation of CDH11 does not impact upstream cascades.

To determine if silencing CDH11 has a significant impact on differentiation under other culturing conditions, cells were grown at different confluencies. As shown in Figure 7A, CDH11 siRNA was applied to low density and high density cells. There were almost no AoAFs with cell-cell contacts in the low density samples, but the majority of cells were in contact with other cells in the high density samples. AoAFs growing at the higher density expressed greater amounts of CDH11, as reported in the literature.[17] Both the low density and high density samples exhibited nearly complete knockdown when treated with CDH11 siRNA, despite the overexpression of CDH11 in the high density case. The αSMA protein expression of the cells was measured, and there was no difference in αSMA protein levels between the untreated samples and treated low density samples (Figure 7B). However, CDH11 siRNA treatment of the cells grown at high density was found to significantly reduce αSMA protein expression (Figure 7B), albeit to a lesser extent than IL1β siRNA treatment (see also Figures 4 and 5). Therefore, CDH11 knockdown is a more promising strategy for attenuating differentiation when the number of AoAF cell-cell contacts is greater.

This finding is particularly important because the *in vivo* environment of the adventitium is crowded, and the cells are densely packed with many cell-cell interactions.[8a] Recent reports in the literature also found CDH11 to be not merely a downstream effector of TGF-β1, but also a factor able to regulate myofibroblast differentiation through multiple other pathways.[17, 42] Moreover, the possible synergistic effects of CDH11 and IL1β knockdown (see Figure 5B) and the role of CDH11 in the propagation *vs.* suppression of maladaptive responses in adventitial fibroblasts (*e.g.*, by coordinating the contraction of fibroblast populations)[10a, 11, 14a] justify further exploration of CDH11 as a possible therapeutic target. Taken together, CDH11 silencing may be a more promising strategy in clinical settings, especially if combined with the knockdown of IL1β.[43]

3. Conclusion

We developed a novel lipid-polymer hybrid formulation to spatiotemporally control the knockdown of key genes implicated in maladaptive responses of human primary adventitial fibroblasts. Our nanocarriers remained dormant in AoAFs until triggered and then silenced protein expression to ≤ 5% of initial levels upon application of a photo stimulus.

Additionally, the dynamics of protein turnover of two functional genes, IL1β and CDH11, were accurately predicted using simple kinetic modeling. This approach allowed the implementation of a double dosing regimen that sustained the knockdown of both genes for one week, which is the time period relevant for severely injured tissue to undergo adventitial remodeling. Cells with silenced IL1β expression for one week exhibited attenuated differentiation and a ~50% reduction in proliferation. The effects of CDH11 knockdown alone were relatively minor, but were significantly enhanced at higher cell densities. However, the combined delivery of IL1β and CDH11 siRNAs resulted in the complete halting of myofibroblast differentiation, as characterized by αSMA expression. Thus, this work provides a new formulation design for imparting stimuli-responsive features into materials capable of transfecting primary cells and elucidated the key functional roles of IL1β and CDH11 in mediating fibrotic responses in AoAFs, both of which are critical for advancing therapies in the clinic to treat cardiovascular disease.

4. Experimental Section

4.1 Materials

Lipofectamine RNAiMAX, anti-CDH11 siRNA, and rabbit IgG polyclonal antibody were purchased from Life Technologies (Carlsbad, CA). Non-targeted (universal negative control) siRNAs were purchased from Sigma-Aldrich (St. Louis, MO). Anti-IL1β siRNA and rabbit IgG polyclonal antibody were obtained from Santa Cruz Biotechnology (Dallas, TX). PAA (M_w = 240,000 g mol^{-1}) was obtained from Acros Organics (Waltham, MA). The mPEG-*b*-P(APNBMA)$_n$ polymers (M_n = 7,900 g mol^{-1}, n = 7.9; M_n = 13,100 g mol^{-1}, n = 23.6) were synthesized *via* atom-transfer radical polymerization as described previously.[46] Dulbecco's Modified Eagle Medium (DMEM) and Dulbecco's phosphate-buffered saline (DPBS, 150 mM NaCl, pH of 7.4) were obtained from Corning Life Sciences – Mediatech Inc. (Manassas, VA). Opti-MEM medium, SuperSignal West Dura Chemiluminescent Substrate, Phalloidin-660, Hoescht 33258, TRIzol Reagent, and AlamarBlue were purchased from Life Technologies (Carlsbad, CA). Antibodies (rabbit anti-GAPDH IgG polyclonal, rabbit anti-αSMA IgG polyclonal, secondary goat anti-rabbit IgG polyclonal-horseradish peroxidase (HRP), and secondary goat anti-rabbit IgG polyclonal-Alexa Fluor 488) and recombinant human TGF-β1 were purchased from AbCam (Cambridge, MA). Bovine serum albumin (BSA) and a bicinchoninic acid (BCA) protein assay kit were purchased from Pierce (Rockford, IL). Primers were obtained from Eurofins MWG Operon (Huntsville, AL) with the following sequences: αSMA forward 5' TATCCCCGGGACTAAGACGG 3'; αSMA reverse 5' CACCATCACCCCCTGATGTC 3'; GAPDH forward 5' CGGGTTCCTATAAATACGGACTGC 3'; GAPDH reverse 5' CCCAATACGGCCAAATCCGT 3'. The iTaq Universal SYBR Green One-Step Kit and optical flat 8-cap strips were purchased from Bio-Rad (Hercules, CA). All other reagents were obtained from Thermo Fisher Scientific (Waltham, MA).

4.2 Formulation of siRNA nanocomplexes

The hybrid nanocomplexes were formed using a solution mixing self-assembly method. Solutions of siRNA and Lipofectamine RNAiMAX were prepared in Opti-MEM and mixed according to Life Technologies' protocol (to produce a final solution containing 0.2 μg

siRNA and 3 μL Lipofectamine in a total volume of 96 μL). After a 5 min incubation period, 0.2 μg 240,000 g mol^{-1} PAA was added to the lipoplex solution. The solution was mixed *via* gentle vortexing and then incubated for 20 min. A separate polymer solution was prepared by adding equimolar amounts of mPEG-*b*-P(APNBMA)$_{7.9}$ and mPEG-*b*-P(APNBMA)$_{23.6}$, on the basis of cationic amine groups. The polymer solution was mixed, *via* gentle vortexing, with the lipoplex/PAA solution to form hybrid complexes with an N:P ratio (N: cationic amine groups on polymer, P: anionic phosphate groups on siRNA) of 4. The hybrid complexes were incubated in a dark environment at room temperature for 30 min prior to further analysis. For the on/off photo-controlled protein silencing experiments, two separate control formulations were used: lipoplexes made with Lipofectamine RNAiMAX according to the manufacturer's protocol and polyplexes formed as described previously.[21]

4.3 Cell culture

Human aortic adventitial fibroblasts were obtained from Lonza (Walkersville, MD) and cultured following Lonza's protocol in stromal cell basal medium (SCBM) supplemented with the stromal cell growth medium (SCGM) SingleQuot Kit. The cells were cultured in a humid environment maintained at 37 °C and 5 vol% CO_2.

4.4 *In vitro* cell transfection

AoAFs were cultured in plates at a density of 15,000 cells cm^{-2} for 24 h. Before transfection, the supplemented growth medium was removed, the cells were washed with DPBS, and Opti-MEM was added to the plates. The nanocomplex solutions were then added dropwise at a final siRNA concentration of 10 nM. Following a 3 h transfection period, the Opti-MEM was replaced with supplemented growth medium for a 30 min recovery period. The medium was replaced with phenol red-free Opti-MEM, and the cells were irradiated with 365 nm light at an intensity of 200 W m^{-2} for 10 min on a 37 °C hotplate. Supplemented growth medium was added to the wells after irradiation. To stimulate cell differentiation in some samples, TGF-β1 was added to the growth medium at a concentration of 10 ng mL^{-1}. The growth medium and TGF-β1 were replenished every two days.

4.5 Protein knockdown analysis

Western blot analyses were used to measure IL1β and CDH11 protein silencing. In the single dose experiments, cells were transfected and lysed at the specified time points. The protein was extracted from the cells by adding a lysis solution composed of 0.5 vol% Triton X-100, 0.5% sodium deoxycholate, 150 mM NaCl, 5 mM Tris–HCl (pH 7.4), 5 mM EDTA, and 1× Halt Protease and Phosphatase Inhibitor cocktail. For the repeated dosing experiments, a second transfection of nanocomplexes was performed 72 h after the first transfection, and protein was extracted at the given time points. The total protein concentration of each sample was measured using the BCA Protein Assay Kit. The protein solutions were subjected to 4% – 20% sodium dodecyl sulfate polyacrylamide gel electrophoresis (SDS-PAGE) for 35 min at 150 V. The separated proteins then were transferred onto a poly(vinylidene fluoride) membrane at 18 V for 75 min. The membrane was subsequently blocked in 5 vol % BSA in Tris–HCl-buffered saline (50 mM Tris–HCl, pH 7.4, 150 mM NaCl) containing 0.1 vol % Tween 20 (TBST) at room temperature for 1 h.

The membrane was incubated overnight with IL1β or CDH11 primary antibodies in TBST at 4 °C. The next day, the membrane was incubated in a solution of secondary antibody conjugated to HRP for 1 h. The SuperSignal West Dura Chemiluminescent Substrate was used to enable detection of the bands through chemiluminescent imaging in a FluorChem Q (ProteinSimple, San Jose, CA). To image the GAPDH bands, the membrane was stripped for 15 min with Restore PLUS Western Blot stripping buffer, blocked in BSA solution for 1 h, and subsequently incubated with GAPDH primary antibody overnight. The next day, after incubation in a solution of secondary goat anti-rabbit antibody conjugated to HRP, chemiluminescent imaging was used to detect the bands. The intensity of each target protein was analyzed with ImageJ software. *Note: A representative western blot image of the anti-IL1β antibody staining is located in* Figure S6.

4.6 RNAi modeling

A set of equations (Equations S1–3) was solved using differential equation solver ode45 in MATLAB.[19] Each siRNA dose was modeled by increasing the normalized siRNA concentration by 100 units following time points corresponding to light-triggered siRNA release. The siRNA turnover rate was estimated by determining the cell doubling time of AoAFs cultured in standard growth medium, which was measured to be ~38 h (Figure S7). Protein degradation rate constants were computed on the basis of IL1β and CDH11 half-lives, which were ~2.5 h and ~8 h, respectively, as reported in the literature.[31] The mRNA degradation rate constants were estimated by using a ~8 h half-life for both genes, as this is the approximate average mRNA turnover rate.[47] Representative MATLAB code is provided in the SI.

4.7 Immunocytochemistry

Cells were transfected with siRNAs. At the specified time points, the cells were washed with DPBS and fixed in 4% paraformaldehyde for 15 min. The cells were permeabilized with 0.1% (v/v) Triton X-100 in DPBS for 15 min and blocked with 5% bovine serum albumin in DPBS for 1 h. αSMA, a marker of myofibroblast differentiation, was detected by overnight incubation at 4 °C in an αSMA primary antibody solution [2 μg mL^{-1} in DPBS]. Alternatively, CDH11 protein expression was detected by overnight incubation at 4 °C in a CDH11 primary antibody solution [2 μg mL^{-1} in DPBS]. Samples were then incubated with a solution of secondary antibody labeled with AlexaFluor® 488 [4 μg mL^{-1} in DPBS] for 1 h. Cells were incubated in a solution of Phalloidin-660 [160 nM in DPBS] for 30 min to detect F-actin, and then the cells were incubated in a solution of Hoescht 33258 [0.5 μg mL^{-1} in DPBS] for 10 min to detect nuclear DNA. Cells were visualized using a 20× objective on an LSM META 510 confocal microscope (Zeiss, Germany) controlled by Image Pro Plus software (version 7.0; Media Cybernetics). The fluorescence intensities in zoomed-out (4× magnification) micrographs were quantified using ImageJ software. The fluorescence intensities of at least 1,000 cells from each channel were averaged through the quantification of total pixel intensity. Then, the signal from the protein of interest (αSMA or CDH11) was divided by the signal from the housekeeping protein (F-actin).

4.8 mRNA knockdown analysis

αSMA mRNA knockdown was measured using quantitative PCR (qPCR). Single and double transfections were carried out, and RNA was isolated by TRIzol Reagent according to the manufacturer's protocols. The iTaq Universal SYBR Green One-Step Kit was used to prepare samples for qPCR in triplicate, using the αSMA or GAPDH primers, as described in the manufacturer's protocols. cDNA synthesis and qPCR were conducted on a Bio-Rad CFX96TM using the following conditions: 10 min at 50 °C; 1 min at 95 °C; 40 cycles of 10 s at 95 °C and 30 s at 60 °C; and finally, a 65 °C to 95 °C ramp at a rate of 0.5 °C every 5 s. The $\Delta\Delta C_T$ method was used for analysis,[48] and all sample data were normalized to data from untreated cell controls.

4.9 Cell Proliferation

Cell growth was evaluated using the AlamarBlue assay according to the manufacturer's protocols. Cells were transfected and grown in fully supplemented medium for 4 days or 7 days after the first transfection for the single dose and double dose experiments, respectively. Medium containing 10 vol% AlamarBlue was added to each well, and the cells were incubated for 6 h in a humid environment maintained at 37 °C and 5 vol% CO_2. Fluorescence was measured using a GloMax-multi detection system plate reader (Promega, Madison, WI). To determine the baseline fluorescence, medium containing 10 vol% AlamarBlue was added to a well without cells. *Note: All samples were treated with the photo-stimulus to isolate the effects of protein knockdown on cellular proliferation*.

Supplementary Material

Refer to Web version on PubMed Central for supplementary material.

Acknowledgments

Work supported by Institutional Development Awards (IDeA) from the National Institute of General Medical Sciences of the National Institutes of Health (NIH) under grant numbers U54-GM104941, P20GM103541, and P20GM10344615. The work also was supported by the National Heart, Lung, and Blood Institute of the NIH under award number R01HL108110. The statements herein do not reflect the views of the NIH. We also acknowledge the Delaware Biotechnology Institute (DBI) and Delaware Economic Development Office (DEDO) for financial support through the Bioscience Center for Advanced Technology (Bioscience CAT) award (12A00448).

References

1. Lloyd-Jones D, Adams RJ, Brown TM, Carnethon M, Dai S, De Simone G, Ferguson TB, Ford E, Furie K, Gillespie C, Go A, Greenlund K, Haase N, Hailpern S, Ho PM, Howard V, Kissela B, Kittner S, Lackland D, Lisabeth L, Marelli A, McDermott MM, Meigs J, Mozaffarian D, Mussolino M, Nichol G, Roger VL, Rosamond W, Sacco R, Sorlie P, Stafford R, Thom T, Wasserthiel-Smoller S, Wong ND, Wylie-Rosett J. Circulation. 2010; 121:e46. [PubMed: 20019324]
2. Motwani JG, Topol EJ. Circulation. 1998; 97:916. [PubMed: 9521341]
3. a) Conte MS. J. Vasc. Surg. 2007; 45:74A.b) Deb S, Cohen EA, Singh SK, Une D, Laupacis A, Fremes SE, Investigators R. J Am Coll Cardiol. 2012; 60:28. [PubMed: 22742399] c) Harskamp RE, Alexander JH, Ferguson TB Jr, Hager R, Mack MJ, Englum B, Wojdyla D, Schulte PJ, Kouchoukos NT, de Winter RJ, Gibson CM, Peterson ED, Harrington RA, Smith PK, Lopes RD. Circulation. 2016; 133:131. [PubMed: 26647082] d) Shavadia J, Norris CM, Graham MM, Verma S, Ali I, Bainey KR. Am Heart J. 2015; 169:833. [PubMed: 26027621]
4. Strauss BH, Rabinovitch M. Am. J. Respir. Cell Mol. Biol. 2000; 22:1. [PubMed: 10615057]

5. Fitzgibbon GM, Kafka HP, Leach AJ, Keon WJ, Hooper GD, Burton JR. J. Am. Coll. Cardiol. 1996; 28:616. [PubMed: 8772748]
6. a) Sousa JE, Costa MA, Abizaid AC, Rensing BJ, Abizaid AS, Tanajura LF, Kozuma K, Van Langenhove G, Sousa A, Falotico R, Jaeger J, Popma JJ, Serruys PW. Circulation. 2001; 104:2007. [PubMed: 11673337] b) Kawatsu S, Oda K, Saiki Y, Tabata Y, Tabayashi K. Ann. Thorac. Surg. 2007; 84:560. [PubMed: 17643635]
7. Weman SM, Salminen US, Penttila A, Mannikko A, Karhunen PJ. Int. J. Legal Med. 1999; 112:107. [PubMed: 10048668]
8. a) Coen M, Gabbiani G, Bochaton-Piallat ML. Arterioscler. Thromb. Vasc. Biol. 2011; 31:2391. [PubMed: 21868702] b) Sartore S, Chiavegato A, Faggin E, Franch R, Puato M, Ausoni S, Pauletto P. Circ. Res. 2001; 89:1111. [PubMed: 11739275]
9. Jiang ZH, Yu P, Tao M, Fernandez C, Ifantides C, Moloye O, Schultz GS, Ozaki CK, Berceli SA. Am. J. Physiol. Heart Circ. Physiol. 2007; 293:H482. [PubMed: 17369455]
10. a) van den Borne SWM, Diez J, Blankesteijn WM, Verjans J, Hofstra L, Narula J. Nat. Rev. Cardiol. 2010; 7:30. [PubMed: 19949426] b) Hutcheson JD, Chen J, Sewell-Loftin MK, Ryzhova LM, Fisher CI, Su YR, Merryman WD. Arterioscler Thromb Vasc Biol. 2013; 33:114. [PubMed: 23162011]
11. Hinz B. J. Invest. Dermatol. 2007; 127:526. [PubMed: 17299435]
12. Braitsch CM, Kanisicak O, van Berlo JH, Molkentin JD, Yutzey KE. J. Mol. Cell. Cardiol. 2013; 65:108. [PubMed: 24140724]
13. Robinson KG, Scott RA, Hesek AM, Woodford EJ, Amir W, Planchon TA, Kiick KL, Akins RE. Bioeng. Transl. Med. 2017 [10.1002/btm2.10060]
14. a) Robinson KG, Nie T, Baldwin AD, Yang EC, Kiick KL, Akins RE Jr. J Biomed. Mater. Res. A. 2012; 100A:1356.b) Nie T, Akins RE Jr, Kiick KL. Acta Biomater. 2009; 5:865. [PubMed: 19167277]
15. Mia MM, Boersema M, Bank RA. PLoS One. 2014; 9
16. Dallon JC, Ehrlich HP. Wound Repair Regen. 2008; 16:472. [PubMed: 18638264]
17. Wang H, Leinwand LA, Anseth KS. FASEB J. 2014; 28:4551. [PubMed: 25008089]
18. Hamm A, Krott N, Breibach I, Blindt R, Bosserhoff AK. Tissue Eng. 2002; 8:235. [PubMed: 12031113]
19. Greco CT, Epps TH III, Sullivan MO. ACS Biomater. Sci. Eng. 2016; 2:1582.
20. Shi Y, Obrien JE, Fard A, Mannion JD, Wang D, Zalewski A. Circulation. 1996; 94:1655. [PubMed: 8840858]
21. Greco CT, Muir VG, Epps TH III, Sullivan MO. Acta Biomater. 2017; 50:407. [PubMed: 28063990]
22. Dominska M, Dykxhoorn DM. J. Cell Sci. 2010; 123:1183. [PubMed: 20356929]
23. Greco CT, Epps TH III, Sullivan MO. J. Vis. Exp. 2017:e55803.
24. Schlegel A, Largeau C, Bigey P, Bessodes M, Lebozec K, Scherman D, Escriou V. J. Control. Release. 2011; 152:393. [PubMed: 21497175]
25. a) Jain S, Kumar S, Agrawal AK, Thanki K, Banerjee UC. Mol. Pharm. 2013; 10:2416. [PubMed: 23597269] b) Aono R, Nomura K, Yuba E, Harada A, Kono K. Biomater. Sci. 2015; 3:764. [PubMed: 26222595]
26. Rezaee M, Oskuee RK, Nassirli H, Malaekeh-Nikouei B. J. Control. Release. 2016; 236:1. [PubMed: 27317365]
27. Goncalves C, Berchel M, Gosselin MP, Malard V, Cheradame H, Jaffres PA, Guegan P, Pichon C, Midoux P. Int. J. Pharm. 2014; 460:264. [PubMed: 24225347]
28. Foster AA, Greco CT, Green MD, Epps TH III, Sullivan MO. Adv. Healthc. Mater. 2015; 4:760. [PubMed: 25530259]
29. Moller K, Muller K, Engelke H, Brauchle C, Wagner E, Bein T. Nanoscale. 2016; 8:4007. [PubMed: 26819069]
30. Germershaus O, Mao SR, Sitterberg J, Bakowsky U, Kissel T. J. Control. Release. 2008; 125:145. [PubMed: 18023906]

31. a) Moors MA, Mizel SB. J. Leukoc. Biol. 2000; 68:131. [PubMed: 10914500] b) Niessen CM, Leckband D, Yap AS. Physiol. Rev. 2011; 91:691. [PubMed: 21527735]
32. Bartlett DW, Davis ME. Nucleic Acids Res. 2006; 34:322. [PubMed: 16410612]
33. Midgley AC, Rogers M, Hallett MB, Clayton A, Bowen T, Phillips AO, Steadman R. J. Biol. Chem. 2013; 288:14824. [PubMed: 23589287]
34. Hecker L, Jagirdar R, Jin T, Thannickal VJ. Exp. Cell. Res. 2011; 317:1914. [PubMed: 21440539]
35. Guo JL, Gu NL, Chen J, Shi TM, Zhou Y, Rong Y, Zhou T, Yang WX, Cui XQ, Chen WH. Arch. Toxicol. 2013; 87:1963. [PubMed: 23640035]
36. a) Kolb M, Margetts PJ, Anthony DC, Pitossi F, Gauldie J. J. Clin. Invest. 2001; 107:1529. [PubMed: 11413160] b) Wilson MS, Madala SK, Ramalingam TR, Gochuico BR, Rosas IO, Cheever AW, Wynn TA. J. Exp. Med. 2010; 207:535. [PubMed: 20176803]
37. Chen H, Yang WW, Wen QT, Xu L, Chen M. Exp. Mol. Pathol. 2009; 87:189. [PubMed: 19747910]
38. a) Bronnum H, Eskildsen T, Andersen DC, Schneider M, Sheikh SP. Growth Factors. 2013; 31:81. [PubMed: 23734837] b) Saxena A, Chen W, Su Y, Rai V, Uche OU, Li N, Frangogiannis NG. J. Immunol. 2013; 191:4838. [PubMed: 24078695]
39. Dewald O, Ren GF, Duerr GD, Zoerlein M, Klemm C, Gersch C, Tincey S, Michael LH, Entman ML, Frangogiannis NG. Am. J. Pathol. 2004; 164:665. [PubMed: 14742270]
40. a) Hinz B, Pittet P, Smith-Clerc J, Chaponnier C, Meister JJ. Mol. Biol. Cell. 2004; 15:4310. [PubMed: 15240821] b) Verhoekx JSN, Verjee LS, Izadi D, Chan JKK, Nicolaidou V, Davidson D, Midwood KS, Nanchahal J. J. Invest. Dermatol. 2013; 133:2664. [PubMed: 23652794]
41. Yoshioka R, Kita Y, Nagahira A, Manno A, Makita N, Tomita U, Murakawa M. J. Pharm. Pharmacol. 2015; 67:1075. [PubMed: 25787991]
42. Chang SK, Noss EH, Chen M, Gu Z, Townsend K, Grenha R, Leon L, Lee SY, Lee DM, Brenner MB. Proc. Natl. Acad. Sci. U.S.A. 2011; 108:8402. [PubMed: 21536877]
43. Vandooren B, Cantaert T, ter Borg M, Noordenbos T, Kuhlman R, Gerlag D, Bongartz T, Reedquist K, Tak PP, Baeten D. Arthritis Rheumatol. 2008; 58:3051.
44. Dzau VJ, Braun-Dullaeus RC, Sedding DG. Nat. Med. 2002; 8:1249. [PubMed: 12411952]
45. Vesey DA, Cheung C, Cuttle L, Endre Z, Gobe G, Johnson DW. J. Lab. Clin. Med. 2002; 140:342. [PubMed: 12434136]
46. Green MD, Foster AA, Greco CT, Roy R, Lehr RM, Epps TH III, Sullivan MO. Polym. Chem. 2014; 5:5535.
47. Schwanhausser B, Busse D, Li N, Dittmar G, Schuchhardt J, Wolf J, Chen W, Selbach M. Nature. 2011; 473:337. [PubMed: 21593866]
48. Schmittgen TD, Livak KJ. Nat. Protoc. 2008; 3:1101. [PubMed: 18546601]

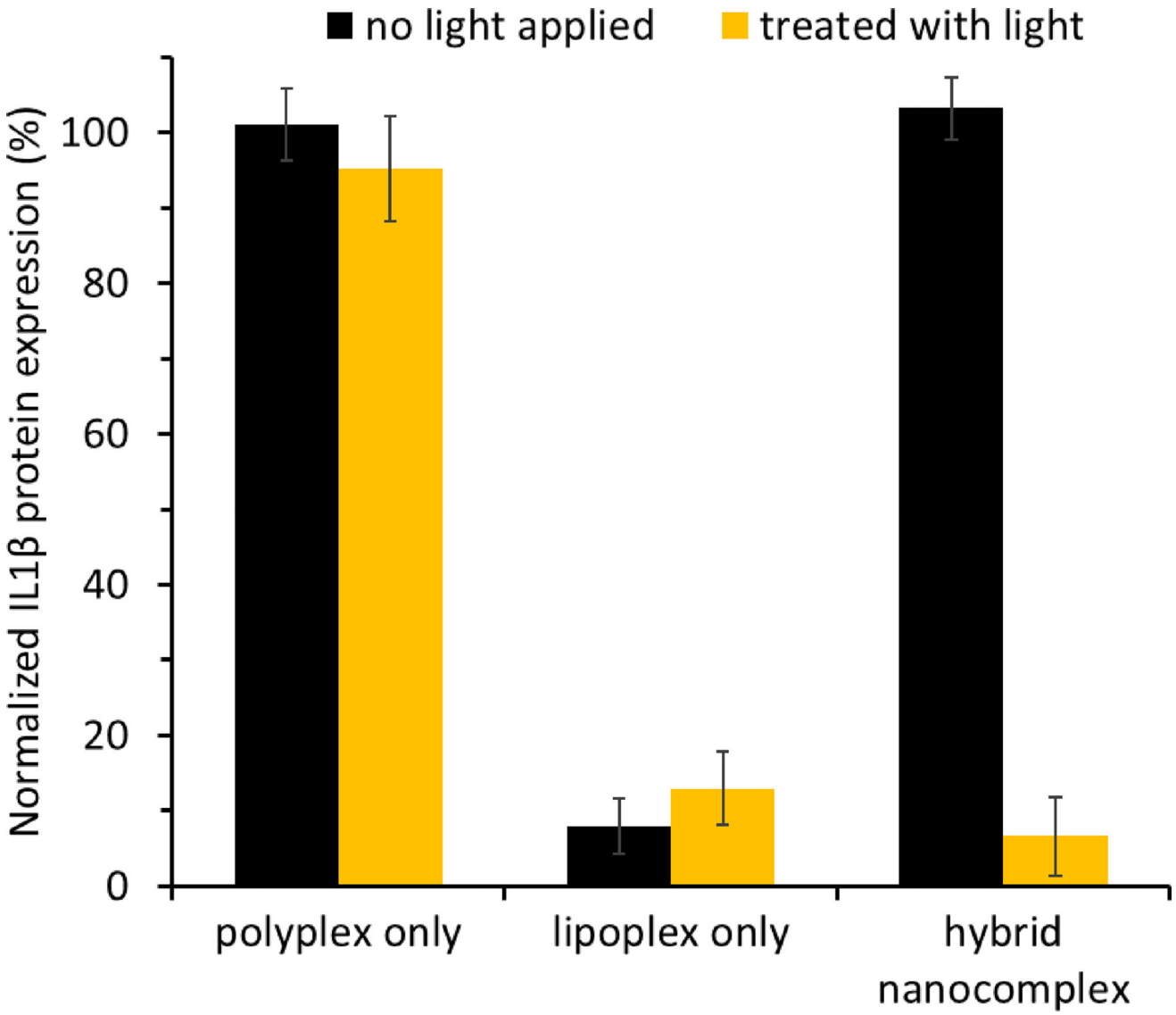

Figure 1.

Photo-controlled IL1β protein silencing with mPEG-*b*-P(APNBMA) polyplexes, Lipofectamine RNAiMAX lipoplexes, and hybrid nanocomplexes. AoAFs were treated with siRNA using the various carriers, irradiated with 365 nm light for either 0 min (black bars) or 10 min (gold bars), and lysed for western blot analysis at 48 h post-transfection. Data represent the IL1β protein expression levels relative to the levels of the loading control glyceraldehyde 3-phosphate dehydrogenase (GAPDH), normalized to the protein levels in controls with no siRNA treatment. Results are shown as the mean ± standard deviation of data obtained from three independent experiments.

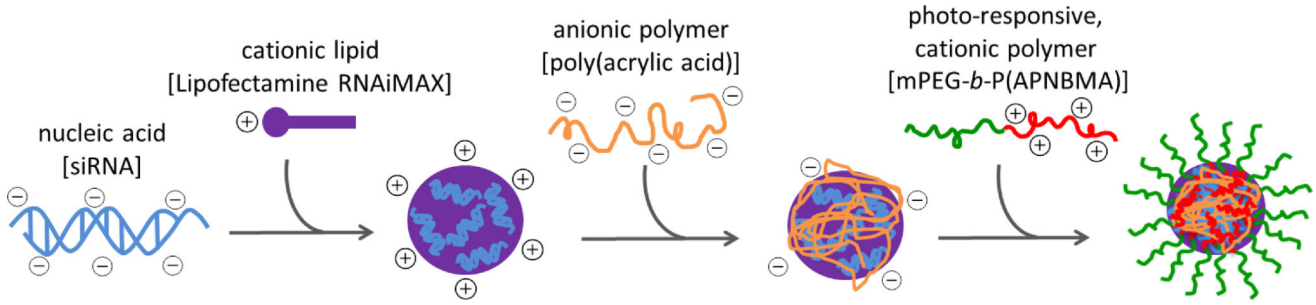

Figure 2.

Schematic depicting the formulation of the hybrid nanocomplexes. First, nucleic acids (siRNA) were encapsulated in lipoplexes using cationic lipid (Lipofectamine RNAiMAX). Second, anionic polymer (PAA) was added to reverse the lipoplexes surface charge. Third, a mixture of photo-responsive cationic polymers (mPEG-*b*-P(APNBMA)$_n$ with 50% n = 7.9 and 50% n = 23.6, on a molar basis of cationic amine groups) was incorporated into the formulation to form the hybrid nanocomplexes.

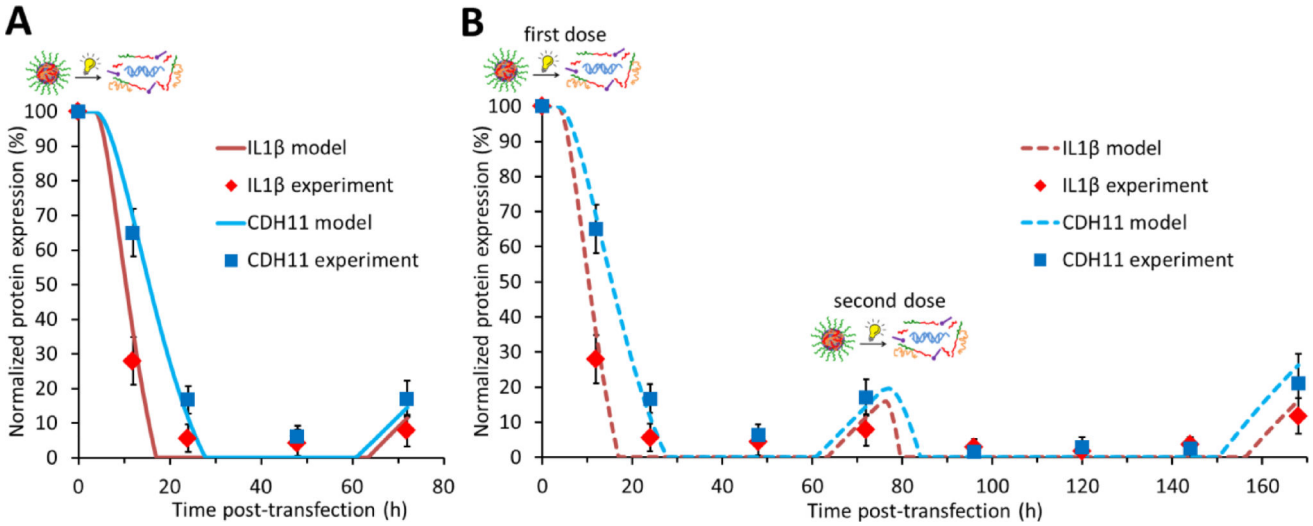

Figure 3.

Dynamics of IL1β and CDH11 protein silencing following a single dose (A) or double dose (B) of siRNA. Kinetic modeling was used to predict the temporal IL1β (dashed red line) and CDH11 (dashed blue line) protein expression following doses of siRNA. Initial protein concentrations were normalized to 100, and the model predictions were verified experimentally using western blotting. Data points represent the normalized IL1β (red diamonds) or CDH11 (blue squares) protein expression levels relative to the loading control. Experimental results are shown as the mean ± standard deviation of data obtained from three independent samples. (A) AoAFs were transfected with the hybrid nanocomplexes at t = 0 h, irradiated with 365 nm light to release the siRNA 3.5 h post-transfection, and lysed at the times indicated by the data points. (B) AoAFs were transfected with the hybrid nanocomplexes at t = 0 h and t = 72 h, irradiated with 365 nm light 3.5 h after each transfection, and lysed at the times indicated by the data points.

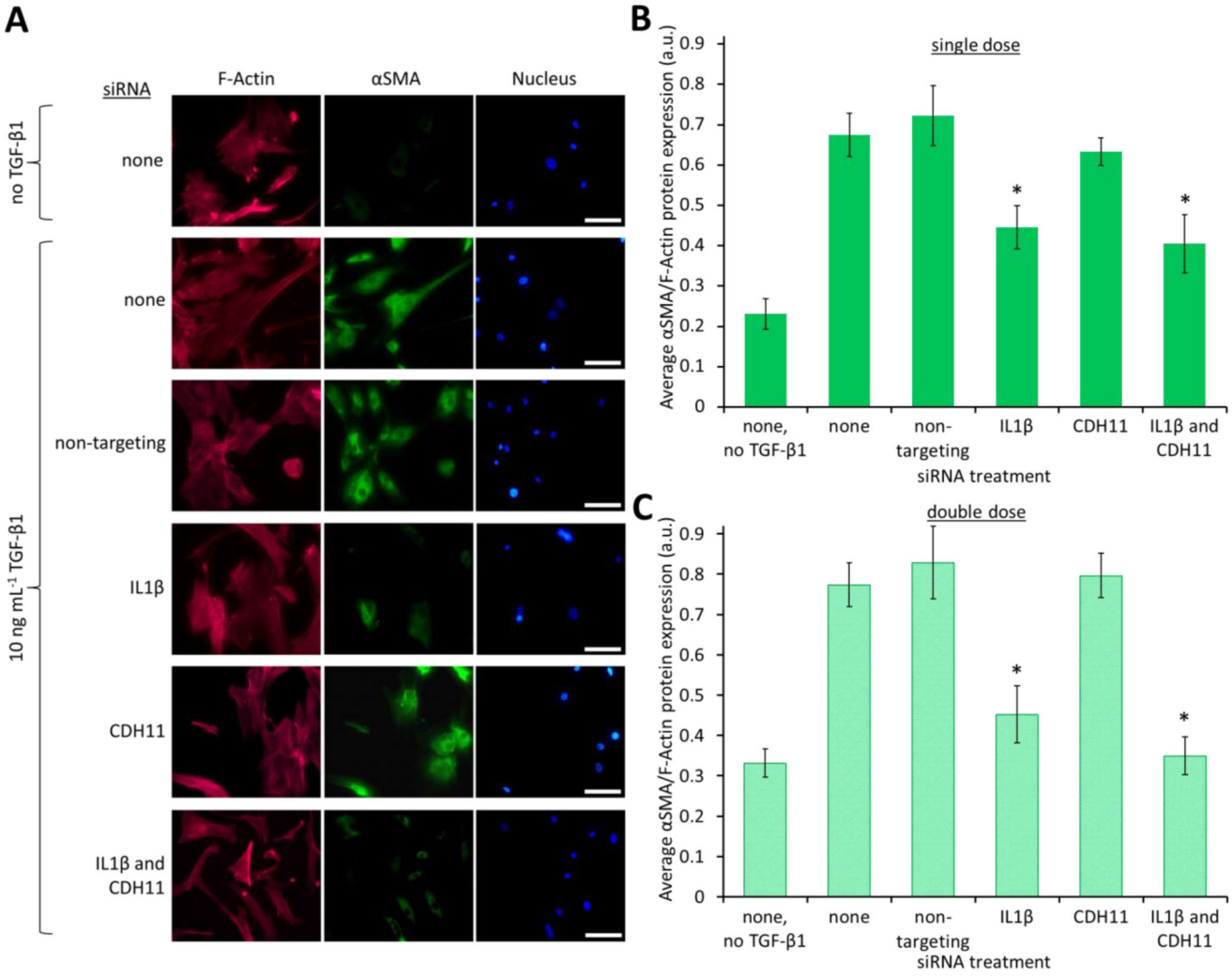

Figure 4.

Attenuation of myofibroblast differentiation (αSMA protein expression) following siRNA dosing. AoAFs underwent transfection with different siRNA formulations and were treated with either 0 or 10 ng mL^{-1} TGF-β1 to induce differentiation. (A) Representative ICC micrographs of AoAFs 4 days post-transfection following a single dose of siRNA. AoAFs were stained for F-actin (magenta), αSMA (green), and nuclear DNA (blue). Scale bars = 50 μm. *Note: A representative zoomed-in micrograph of F-actin staining showing stress fibers is located in* Figure S4. (B) Quantification of relative αSMA protein expression from single dose ICC micrographs in (A). (C) Quantification of relative αSMA protein expression from double dose ICC micrographs [not shown], characterized on day 8. The average total fluorescence intensity of αSMA relative to F-actin of at least 100 cells per sample was measured using ImageJ for both the single and double dose regimens. All results are shown as the mean ± standard deviation of data obtained from three independent experiments. An asterisk indicates a statistically significant difference in αSMA protein expression in comparison to the no siRNA and 10 ng mL^{-1} TGF-β1 treatment control ($p < 0.05$).

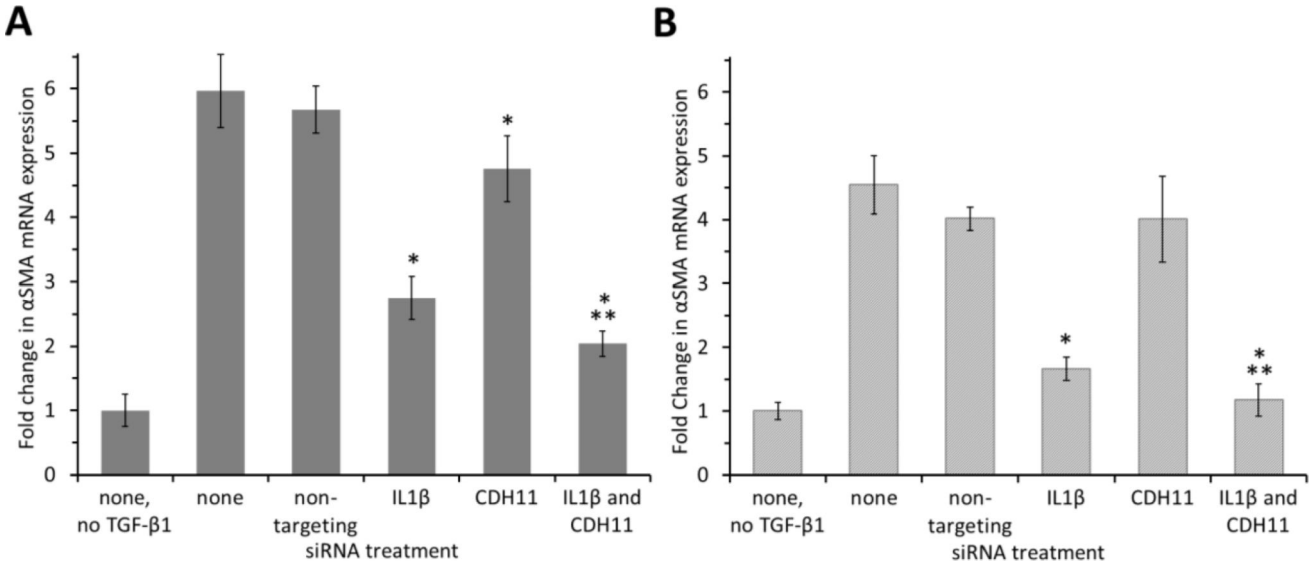

Figure 5.

Attenuation of myofibroblast differentiation (αSMA mRNA expression) following the two different siRNA dosing schedules. AoAFs underwent transfection at either t = 0 h (A) or t = 0 h and t = 72 h (B) with various siRNA formulations and were treated with either 0 or 10 ng mL^{-1} TGF-β1 to induce differentiation. (A) qPCR analyses of αSMA mRNA expression levels 3 days post-transfection in the single dose regimen. (B) qPCR analyses of αSMA mRNA expression levels 7 days after the first transfection [4 days after the second transfection] in the double dose regimen. qPCR values were normalized to the levels in the no siRNA and no TGF-β1 treatment control for each dosing schedule. All results are shown as the mean ± standard deviation of data obtained from three independent samples. A single asterisk indicates a statistically significant difference in αSMA mRNA expression in comparison to the no siRNA and 10 ng mL^{-1} TGF-β1 treatment control, and a double asterisk indicates a statistically significant difference in αSMA mRNA expression in comparison to the IL1β siRNA treatment formulation ($p < 0.05$).

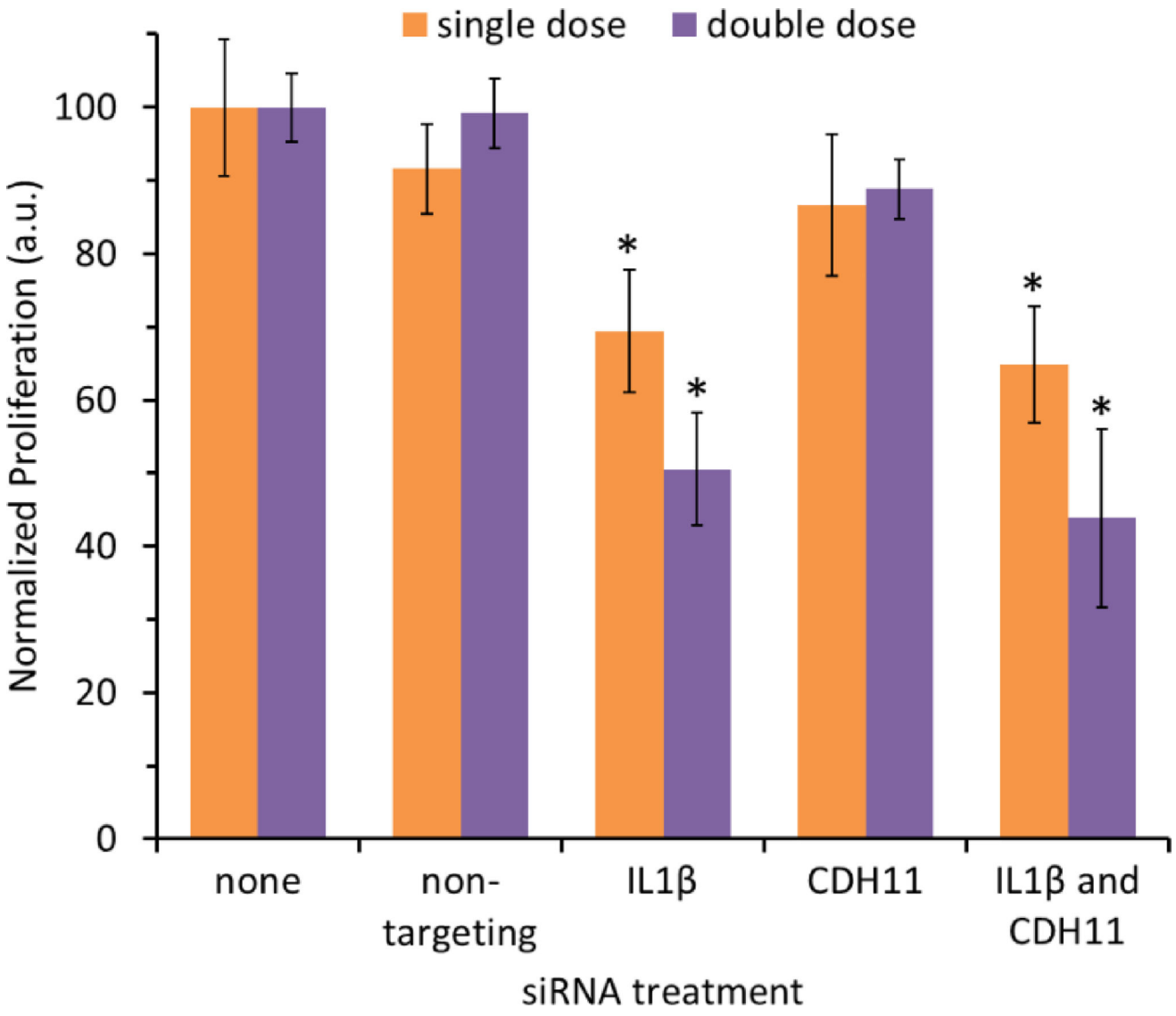

Figure 6.

Proliferation of AoAFs following the single or double dose siRNA regimen. AoAFs were treated with different siRNA formulations and irradiated with 365 nm light for 10 min after each transfection. The change in the number of cells was measured using the AlamarBlue assay 4 days or 7 days after the first transfection for the single dose (orange bars) and double dose (purple bars) experiments, respectively. Data represent the normalized extents of cellular proliferation relative to cells that were not treated with siRNA, with 100 indicating no change relative to untreated cells. A value of 0 indicates no change in the absolute number of cells from the time of transfection. Results are shown as the mean ± standard deviation of data obtained from three independent experiments. An asterisk indicates a statistically significant difference in proliferation in comparison to the no siRNA treatment controls ($p < 0.05$).

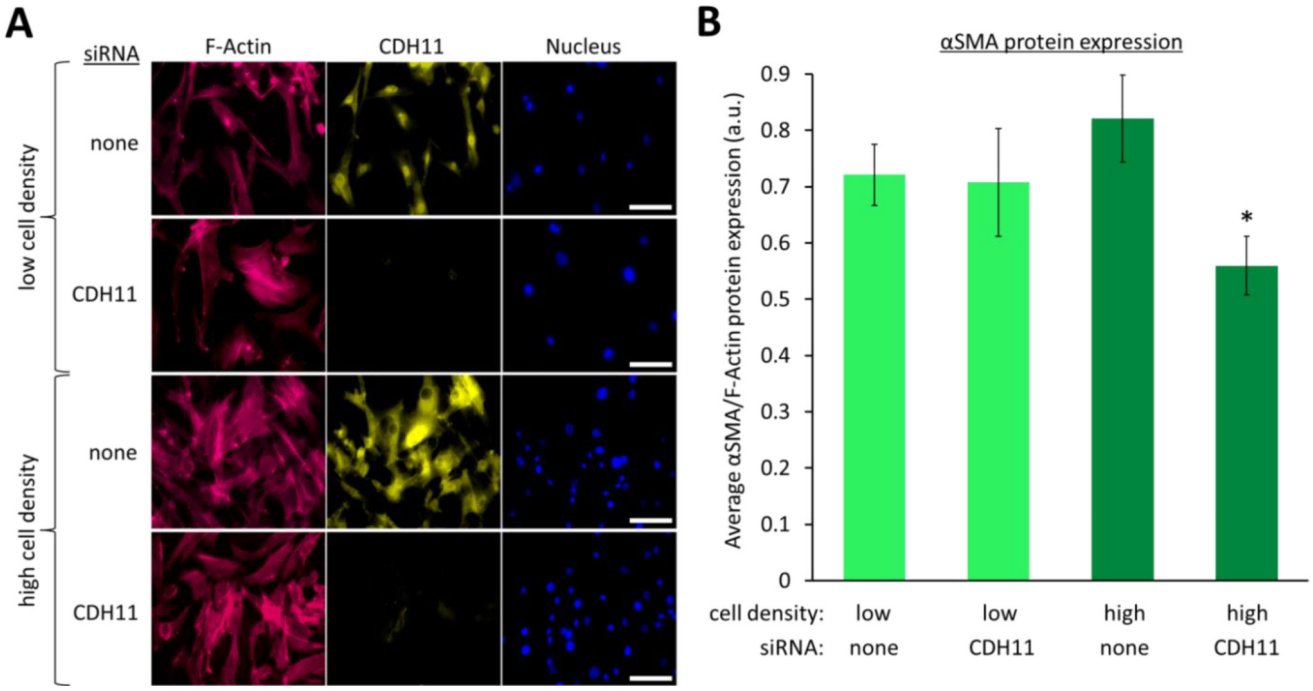

Figure 7.

Effect of cell density on myofibroblast differentiation following CDH11 knockdown. AoAFs were plated at 10,000 cells cm^{-2} (low density) or 30,000 cells cm^{-2} (high density), transfected with CDH11 siRNA, and treated with 10 ng mL^{-1} TGF-β1 to induce differentiation. ICC analyses were conducted to measure (A) CDH11 or (B) αSMA protein expression. (A) Representative ICC micrographs of AoAFs 2 days post-transfection. AoAFs were stained for F-actin (magenta), CDH11 (yellow), and nuclear DNA (blue). Scale bars = 50 μm. (B) Quantification of αSMA protein expression from ICC analyses. The average total fluorescence intensity of αSMA relative to F-actin of at least 100 cells per sample was measured using ImageJ. Results are shown as the mean ± standard deviation of data obtained from three independent samples. An asterisk indicates a statistically significant difference in αSMA protein expression in comparison to the no siRNA treatment control at the appropriate cell density ($p < 0.05$).